Research on the thermohydraulic performance of parallel evaporative cooling system for Insulated Gate Bipolar Transistor

Yitao Shi[1,2*], Aili, Zhang[1], Zhanchuan Wu[1,2]

[1] School of Mechanical and Equipment Engineering, Hebei University of Engineering, Handan, 056038, China
2: Key Laboratory of Intelligent Industrial Equipment Technology of Hebei Province
Email: shiyitao@hebeu.edu.cn

Abstract: Thermohydraulic performance of the parallel evaporative cooling system (PECS) is quite essential for the efficient and safe operation of IGBT modules. This paper aims to develop a novel coupling model of PECS for optimal design. The thermohydraulic coupling performance of the PECS is analyzed from the perspectives of two-phase flow and heat transfer. The influence of the thermal flux, branch diameter, and number of parallel evaporators on temperature and flow distribution of the PECS is thoroughly studied. The findings indicate that the high thermal flux will alter the flow pattern in the evaporator, resulting in a wall temperature jump. The thermal flux has a great influence on the flow distribution, and the maximum deviation between the evaporator is 30%. The branch diameter does not affect the temperature distribution of PECS, while the branch diameter has a great influence on the flow distribution. The minimum critical branch diameter of the PECS for efficient operation is 6 mm. The number of parallel evaporators significantly influences the thermohydraulic performance. The number of parallel evaporators suitable for optimal thermohydraulic performance of PECS is less than 12. The 24 parallel evaporators are the maximum number to ensure the uniform flow distribution of the PECS.
Key words: IGBT, Evaporative cooling, Thermohydraulic, HTC, Flow distribution

1. Introduction

Global warming has become a global challenge. In response to the pressures of climate change, many countries are proposing carbon-neutral energy policies aimed at accelerating the transition to clean energy. Wind energy has become one of the most widely used renewable energy sources[1]. As the core of wind power conversion, the Insulated Gate Bipolar Transistor (IGBT) is developing in the direction of high-power density[2]. The average thermal flux of the IGBT module is as high as 500 W/cm^2, which brings serious challenges to its cooling[3]. The overtemperature phenomenon of the IGBT module occurs frequently, which leads to the failure of the whole wind power conversion. Therefore, it is crucial to develop an efficient cooling system to ensure the safe and reliable operation of the IGBT module[4]. The evaporative cooling system relies on coolant evaporation to realize the efficient cooling of the IGBT module. The system has the advantages of high efficiency, uniform temperature distribution, and high reliability, and has become one of the most promising IGBT cooling technologies.

The performance of PECS is affected by the flow distribution between the evaporators[5, 6]. Li et al. [7] assessed the influence of flow distribution on the performance of a plate heat exchanger, and the research results showed that the two-phase refrigerant flow maldistribution would lead to a 29.8% decline in the performance of the heat exchanger. The maldistribution is influenced by various factors, which can be classified into three primary types: operating conditions, fluid properties, and geometrical factors[8-10]. Yang et al. [11] investigated the impact of fluid characteristics on refrigerant distribution by comparing the results of R245fa, R134a, R410A, and R32. The research findings showed that R245fa displayed the most favorable distribution with low vapor and high liquid densities. Liu et al. [12] investigated the phase distribution of vapor-liquid slug flow in six parallel micro-channels with different branch distances. They discovered that the characteristics of phase distribution in two-phase flow within parallel channels significantly rely on the inlet flow conditions and the spacing between the channels. Huang et al. [13] conducted a visual study on the uniformity of flow distribution in parallel multi-channel. The findings indicated that changing the position of the coolant entering the parallel channel

can greatly promote the uniformity of flow distribution. Wang et al. [14] proposed a biomimetic IGBT parallel cooling system in which foam metal was added between parallel channels. The experimental results showed that the flow distribution became more uniform between parallel channels. Gao et al. [15] analyzed the non-uniform flow distribution and non-uniform heat transfer in parallel microchannels. Through the optimization of the location and injection angle of the manifold inlet, researchers found that it was able to increase the thermal capacity in the high thermal flux region and improve the uniformity of temperature in the substrate.

Several mechanism models have been made to comprehend the flow distribution characteristics of the parallel system[16, 17]. Oevelen et al. [18] presented a two-phase flow distribution model that focuses on the distribution of flow rate in hundreds of parallel pipes. The model assessed the influence of the inlet temperature, heat flux, velocity, and other factors on the flow maldistribution. Xu et al. [19] established a cooling system model with 55 pipes in parallel, utilizing the VOF and k-ω turbulence models. The model can better reflect the flow distribution in each channel under different inlet qualities. Qiao et al. [20] established a manifolds-channels simulation model, and the influence of channel array dimension, channel length, and inlet header diameter was analyzed. The system performance is optimized by using the machine learning method. The results showed that the system flow non-uniformity is reduced by 93.39%. Hussein et al. [21] established a novel circular heat exchanger model with L-shaped parallel channels. The results showed that this arrangement could significantly reduce the coolant misdistribution and improve the heat transfer capacity of the heat exchanger.

The literature review indicates that the performance of the PECS has received some attention, and some flow distribution models have been established. However, there has been limited exploration of the thermohydraulic coupling performance of PECS for IGBT. Therefore, this study aims to develop a novel coupling model of PECS. An experimental setup of PECS is established to validate the accuracy of the proposed model. The thermohydraulic coupling performance of the PECS is analyzed from two-phase flow and heat transfer perspectives. Furthermore, the influence of the thermal flux, branch diameter, and number of parallel evaporators on temperature and flow distribution of the PECS is thoroughly studied. The optimal design boundary of the system is given, which provides a theoretical foundation for the optimal design of the PECS for IGBT.

2. Numerical model

A schematic of PECS is presented in Fig. 1. The system consists of IGBT, evaporator, condenser, collecting manifold, dividing manifold, riser, downcomer, and branches, among them, a copper heater is used to simulate the heat generated by the transistor in the IGBT. First, the heat generated by the IGBT is conducted to the wall of the evaporator. Secondly, the coolant is heated and evaporated in the evaporator, forming a vapor-liquid mixture. Again, the buoyancy forces drive this mixture into the branches and the collecting manifold, after which it flows through the riser into the condenser for vapor condensation. Finally, the resulting liquid then passes through the downcomer into a dividing manifold, where it is redistributed to each evaporator to restart the next cycle. The PECS relies on gravity for natural circulation cooling. Detailed dimensions are provided in Table 1.

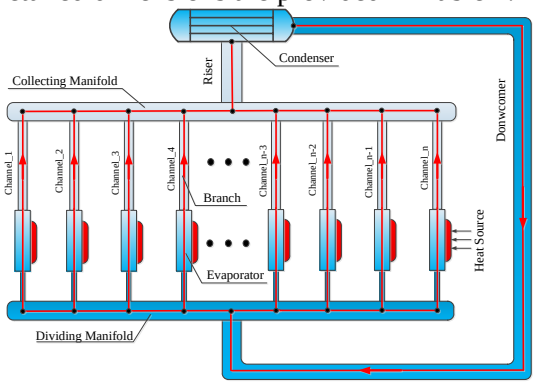

Fig. 1. Schematic of the PECS

Table 1. Geometrical parameter

Name	Unit	Value
Riser diameter	mm	30
Riser length	mm	600
Downcomer diameter	mm	30
Downcomer length	mm	3000
Collecting manifold diameter	mm	30
Channel interval	mm	800
Dividing manifold diameter	mm	30
Evaporator height	mm	140
Evaporator width	mm	130
Evaporator thickness	mm	26

Furthermore, this model is divided into the evaporator model and pipeline model according to whether there is heat transfer in the component. The novel coupling model of PECS will be developed based on the lumped parameter method. The evaporator is discretized based on the evaporation initiation of the coolant. The pipeline model includes the manifold, downcomer, and riser, which are discretized by nodes of tubes. The coolant condition is determined at each node based on temperature and pressure, which does not account for the impact of pressure drop on the physical properties of the fluid. Besides, the loss of friction, kinetic energy, and viscous dissipation is not considered during the coolant flow. The mass velocity, pressure, and enthalpy are solved with three conservation equations.

Mass conservation: $$\frac{\partial G}{\partial z} = 0 \tag{1}$$

Momentum conservation: $$\frac{\partial G^2}{\rho \partial z} = -\partial p_f - \frac{\partial p}{\partial z} - \partial p_g \tag{2}$$

Energy conservation : $$\partial Q = \frac{\partial GH}{\partial z} \tag{3}$$

2.1. Evaporator model

A schematic of the evaporator is presented in Fig. 2. The thermal flux q from the IGBT to the evaporator is evaluated by the Newton cooling formula. According to the heat absorption of coolant in the evaporator, the flow of coolant is separated into two sections: preheating and evaporation. Each section exit enthalpy H_{i+1} is calculated using energy balance. The single-phase heat transfer coefficient (HTC) α_l of preheating is calculated with the Dittus-Boelter correlation. The HTC α_{tp} of evaporation is determined using the Gungor and Winterton correlation[22].

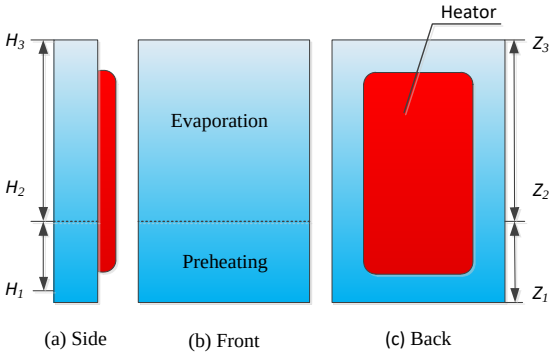

Fig. 2. Schematic of evaporator

$$H_{i+1} = H_i + \frac{q}{GA}(z_{i+1} - z_i)w \tag{4}$$

$$\alpha_l = 0.023 \mathrm{Re}_l^{0.8} \mathrm{Pr}_l^{0.4} \frac{k_l}{D} \tag{5}$$

$$\alpha_{tp} = R\alpha_b + E\alpha_l \tag{6}$$

$$\alpha_b = \frac{55 q^{0.67} p_r^{0.12}}{\sqrt{M}} \left(0.4343 \ln \frac{1}{p_r}\right)^{-0.55} \tag{7}$$

$$q = \alpha_i (T_w - T_i) \tag{8}$$

Where q is thermal flux (W/m^2), α is HTC ($W/m^2 \cdot K$), H is enthalpy (kJ/kg), G is mass velocity ($kg/(m^2 \cdot s)$), w is evaporator width (m), A is cross sectional area of evaporator (m^2), z is the length of the coolant flowing in the evaporator (m), T is temperature (K), k is thermal conductivity ($W/m \cdot K$), Pr is Prandtl number, Re is Reynolds number, D is diameter (m), R and E correlation constant, p_r is reduced pressure, M is molecular weight (kg/kmol). Subscripts: *i* is node number, w is wall, l is liquid phase, and tp is two-phase.

According to the momentum balance, the pressure drop in preheating consists of frictional resistance Δp_{l_f} and gravity-induced pressure drop Δp_{l_g}. In evaporation, the pressure drop includes acceleration pressure drop Δp_a, frictional resistance Δp_{tp_f}, and gravity-induced pressure drop Δp_{tp_g}, in which the frictional resistance adopts the separated flow model. The frictional multiplier adopts the Friedel correlation[23], and the slip ratio is given by using Miropolskii correlation[24].

Preheating model:

$$p_{i+1} = p_i - \Delta p_{l\_f} - \Delta p_{l\_g} \tag{9}$$

$$\Delta p_{l\_f} = \frac{\lambda_l G^2 \upsilon_l}{2D} \Delta z \tag{10}$$

$$\Delta p_{l\_g} = \rho_l g \Delta z \tag{11}$$

$$\text{when } \mathrm{Re}<2300,\ \lambda_l = 64 \mathrm{Re}^{-1} \tag{12}$$

$$\text{when } \mathrm{Re}>2300,\ \lambda_l = 0.3164 \mathrm{Re}^{-0.25} \tag{13}$$

Evaporation model:

$$p_{i+1} = p_i - \Delta p_a - \Delta p_{tp\_f} - \Delta p_{tp\_g} \tag{14}$$

$$\Delta p_{tp\_f} = \frac{\lambda_l G^2 \upsilon_l}{2D} \phi_{lo}^2 \Delta z \tag{15}$$

$$\phi_{lO}^2 = (1-x)^2 + x^2 \frac{\rho_l}{\rho_v} \frac{\lambda_v}{\lambda_l} + 3.24 \left(\frac{\upsilon_\upsilon}{\upsilon_l}\right)^{0.91} \frac{\left(\frac{\mu_v}{\mu_l}\right)^{0.19} \left(1 - \frac{\mu_v}{\mu_l}\right)^{0.7} x^{0.78} (1-x)^{0.24}}{\mathrm{Fr}_{lo}^{0.045} \mathrm{We}_{lo}^{0.035}} \tag{16}$$

$$\varphi = \frac{1}{1 + S\frac{\rho_v}{\rho_l}\frac{1-x}{x}} \tag{17}$$

$$S = 1 + \frac{13.5}{Fr_{lo}^{5/12} Re_{lo}^{1/6}}\left(1 - \frac{p}{p_{cr}}\right) \tag{18}$$

$$\Delta p_a = G^2 \upsilon_l \left(\frac{x^2}{\varphi}\left(\frac{\upsilon_\upsilon}{\upsilon_l}\right) + \frac{(1-x)^2}{(1-\varphi)} - 1\right) \tag{19}$$

$$\Delta p_{tp\_g} = (\rho_\upsilon \varphi + \rho_l (1-\varphi)) g \Delta z \tag{20}$$

Where p is pressure (Pa), λ is friction factor, v is specific volume (m^3/kg), x is vapor quality, φ is void fraction, ϕ is frictional multiplier, S is slip ratio, Fr is Froude number, We is Weber number, g is gravity acceleration (m/s^2), ρ is density (kg/m^3), μ is dynamic viscosity (Pa·s). Subscripts: v is vapor phase, lo is only liquid.

2.2. Pipeline model

A schematic of pipeline is presented in Fig. 3. The pipeline model includes collecting manifold, dividing manifold, downcomer, and riser (branch) model. When the coolant flows in these pipelines, there is no heat transfer between the coolant and the surface pipe. Thus, the flow process is considered as adiabatic flow approximately. The pressure drop in the collecting manifold, branch, and riser consists of two-phase flow frictional pressure drop and gravity pressure drop. The pressure drop in the dividing manifold and downcomer includes single-phase flow frictional pressure drop and gravity pressure drop. In addition, the pipeline model also includes the sudden expansion and sudden contraction of the resistance pressure drop at the inlet and outlet of the evaporator. The detailed model is as follows.

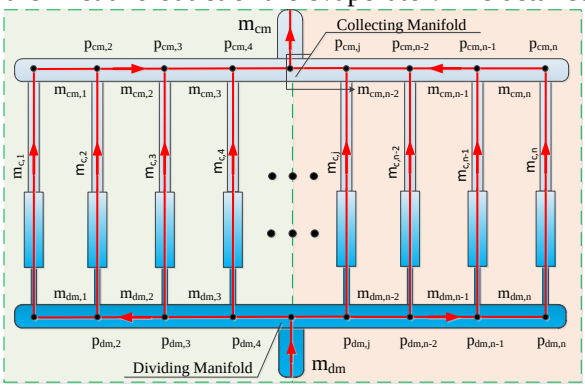

Fig. 3. Schematic of pipeline

Manifold model:

$$m_{cm,i+1} = m_{cm,i} + m_{c,i+1} \tag{21}$$

$$p_{cm,i-1} - p_{cm,i} = \lambda \frac{(G_{cm,i-1})^2 \upsilon_l}{2D} \phi_{lo,i-1}^2 z_{cm,i} \tag{22}$$

$$m_{dm,i+1} = m_{dm,i} + m_{c,i} \tag{23}$$

$$p_{dm,i+1} - p_{dm,i} = \lambda_l \frac{(G_{dm,i})^2 \upsilon_l}{2D} z_{dm,i} \tag{24}$$

Riser (branch) model:

$$\Delta p_r = \frac{\lambda_l G_r^2}{2D\rho_l}\phi_{lo}^2 L_r + (\rho_v \varphi + \rho_l(1-\varphi))g z_r \quad (25)$$

Downcomer model:

$$\Delta p_d = \frac{\lambda_l G_d^2}{2D\rho_l} L_d + \rho_l g z_d \quad (26)$$

Sudden contraction:

$$\Delta p_c = \frac{G_d^2}{\rho_l} a(1-a) \quad (27)$$

Sudden enlargement:

$$\Delta p_e = \frac{G_d^2}{2\rho_l}[(\frac{1}{C_c}-1)^2 + (1-\frac{1}{a^2})][1+(\frac{\rho_l}{\rho_{lg}})x] \quad (28)$$

Where m is the mass flow rate of branch (kg/s), Δp_r is the pressure drop of riser (Pa), Δp_d is the pressure drop of downcomer(Pa), L_r and z_r are length and height of riser (m), respectively, L_d and z_d are length and height of downcomer (m), respectively, a is the cross-sectional ratio, C_C is contraction ratio. Subscripts: cm is collecting manifold, dm is dividing manifold.

2.3. Model validation

An experimental setup of PECS is established to validate the accuracy of the proposed model. The whole system includes evaporator, manifold, riser, downcomer, condenser, heater instead of IGBT transistor, data collector, and other main components, as shown in Fig. 4. The geometric parameters of primary equipment are detailed in Table 2. During the testing, the thermal flux of the heater increases from 10 kW/m^2 to 45 kW/m^2, while the system pressure is maintained at approximately 10 kPa. The experimental data of the wall temperature of the evaporator and the inlet mass velocity of the evaporator are recorded for comparison with the prediction results.

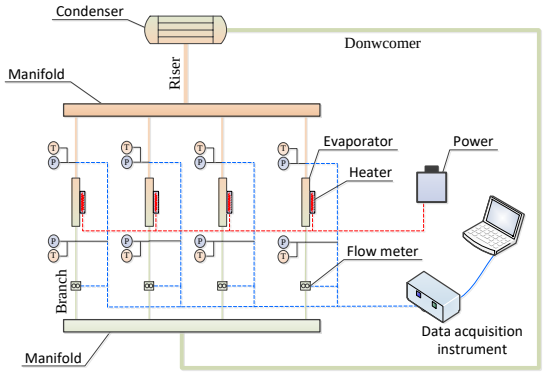

Fig. 4. Experimental device of PECS

Table 2. Geometric parameter

Parameter	Unit	Value
Height of evaporator	mm	140
Length of evaporator	mm	130
Width of evaporator	mm	30
Diameter of manifold	mm	30
Diameter of downcomer	mm	12
Diameter of riser	mm	12

The comparison of the predictions with the experimental values of PECS is shown in Fig. 5. The deviations in wall temperature and mass velocity for evaporators #1-#4 are less than 10 %. The results indicate a high agreement between the predictions and the experimental data. Thus, the proposed model

accurately reflects the thermohydraulic performance of PECS. The subsequent analysis and discussions can be carried out based on the coupling model.

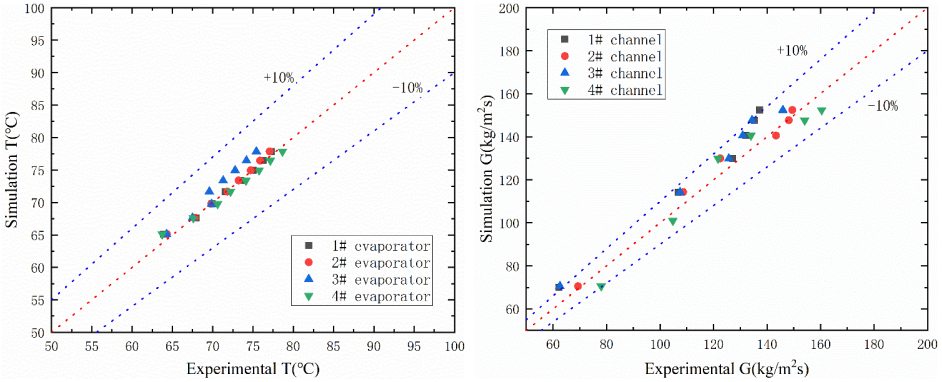

(a) Wall temperature (b) Mass velocity

Fig. 5. Comparison of the predictions with the experimental data.

3. Results and discussion

The thermohydraulic performance of PECS is analyzed by changing the thermal flux, the branch diameter, and the number of parallel evaporators. Specifically, the thermal flux ranges between 20.4 kW/m^2 and 40.8 kW/m^2, the channel diameter varies between 4 mm and 12 mm, and the number of parallel evaporators adjusts between 4 and 24. Detailed parameters are shown in the Table. 3. The temperature distribution is quantified through wall temperature and HTC, whereas the flow distribution is analyzed using mass velocity and quality.

Table 3. Boundary condition for PECS

Design variation	q (kW/m^2)	D (mm)	N
Thermal flux	20.4	12	22
	25.5	12	22
	30.6	12	22
	35.7	12	22
	40.8	12	22
Branch diameter	25.5	4	22
	25.5	6	22
	25.5	8	22
	25.5	10	22
	25.5	12	22
	25.5	14	22
Number of parallel evaporators	25.5	12	4
	25.5	12	8
	25.5	12	12
	25.5	12	16
	25.5	12	20
	25.5	12	24

3.1. Thermohydraulic performance

The influence of thermal flux, branch diameter, and number of evaporators on the thermohydraulic of PECS is shown in Figs. 6-8. In Fig. 6, as the thermal flux increases from 20.41 kWm^{-2} to 30.61 kWm^{-2}, the temperature gradually increases, while the mass velocity shows the opposite trend. When the thermal flux increases to 35.71 kWm^{-2}, the wall temperature decreases to approximately 65 ℃, indicating a strengthening of evaporation in the evaporator. However, when the thermal flux further increases from 35.71 kWm^{-2} to 40.82 kWm^{-2}, the temperature appears a rapid jump to about 77 ℃ and the mass velocity decreases significantly. This phenomenon can be attributed to the sharp increase of bubble growth in the evaporator, which results in a decline in heat transfer efficiency. Therefore, the results indicate that the transition of the two-phase flow pattern from slug flow to mist flow in the evaporator.

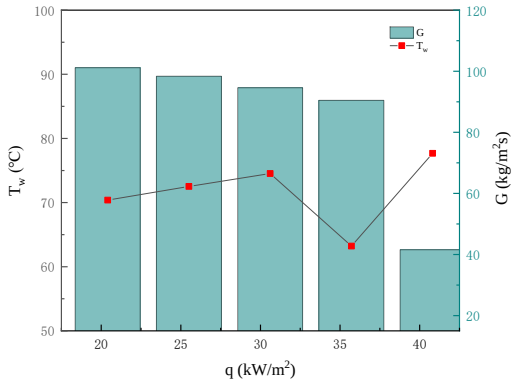

Fig. 6. Effect of the thermal flux on thermohydraulic performance.

When the branch diameter increases, the wall temperature decreases and the mass velocity gradually increases in Fig. 7. It is worth noting that a significant wall temperature decrease of 10 °C is recorded when the branch diameter is increased to 8 mm. This indicates a significant reduction in the circulating resistance of the PECS, resulting in enhanced heat transfer in the evaporator. When the branch diameter exceeds 8 mm, the branch diameter continues to increase, the mass velocity increases slowly, and the wall temperature hardly decreases. This indicates that increasing the branch diameter does not further improve the thermohydraulic performance of the PECS. Therefore, the branch diameter of 8 mm is determined to be the minimum critical branch diameter for the highly efficient operation of PECS.

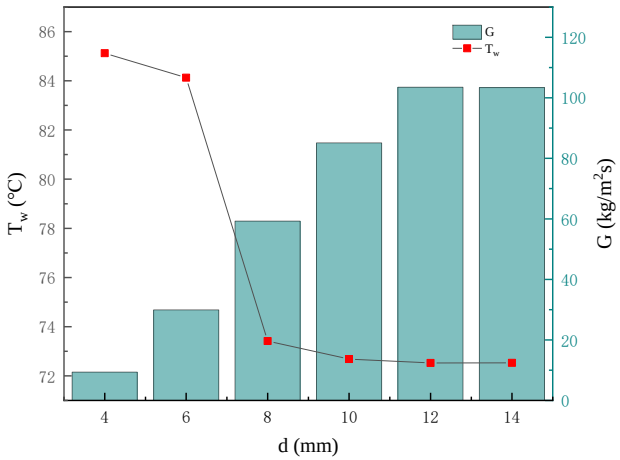

Fig. 7. Effect of the branch diameter on thermohydraulic performance.

In Fig. 8, as the number of parallel evaporators increases, the wall temperature and mass velocity show opposite changes. When the number of parallel evaporators increases, the wall temperature and flow mass velocity change rate increase rapidly, which shows that the number of parallel evaporators has a great impact on the thermohydraulic performance. Significantly, when the number of parallel evaporators exceeds 12, the temperature increases by more than 0.2 ℃, and the mass velocity decreases by more than 10 kg/m^{2}s. It is mainly due to the increase in parallel evaporator leads to a rapid increase in circulation resistance of PECS. Thus, the number of parallel evaporators suitable for PECS is less than 12.

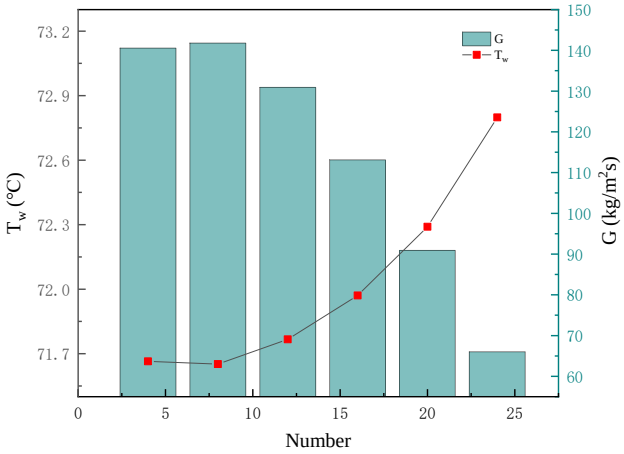

Fig. 8. Effect of the number of parallel evaporators on thermohydraulic performance.

3.2. Temperature and flow distribution

3.2.1 Effect of the thermal flux

When the thermal flux changes between 20.41 kWm^{-2} and 30.61 kWm^{-2}, the wall temperature shows a highly uniform distribution between each evaporator in Fig. 9(a). The wall temperature presents an uneven distribution at 35.71 kWm^{-2}, but the range of this change is within 2 ℃. Thus, the influence of thermal flux on wall temperature distribution is weak. The distribution of HTC in different evaporators is shown in Fig. 9(b). When the thermal flux is lower than 25.51 kWm^{-2}, the HTC distribution between different evaporators is more uniform; when the thermal flux is more than 25.51 kWm^{-2}, the HTC of Numbers 10-15 evaporators is significantly higher. Therefore, this shows that high thermal flux has an obvious influence on the distribution of HTC.

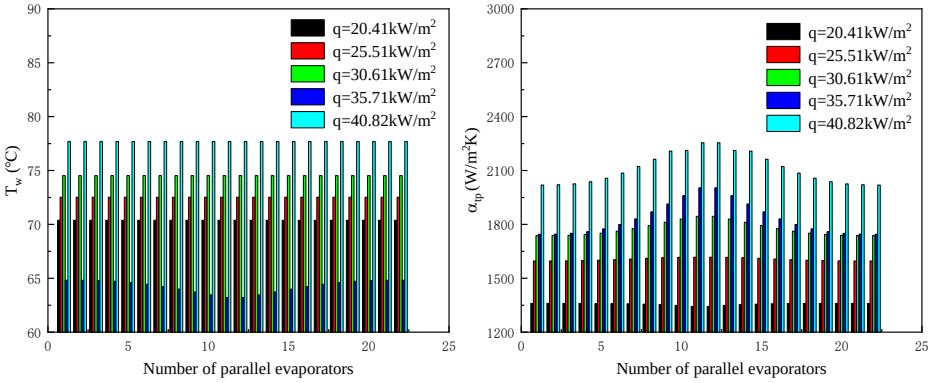

(a) Wall temperature (b) HTC

Fig. 9. Effect of the thermal flux on temperature distribution.

The mass velocity shows a very uneven distribution in Fig. 10(a). As the thermal flux increases from 35.71 kWm^{-2} to 40.82 kWm^{-2}, the maldistribution between parallel evaporators is getting worse. At a thermal flux of 40.82 kWm^{-2}, the maldistribution is the largest, with a maximum deviation of 30.71 %. The reason for this result is that the rapid increase in thermal flux leads to a sharp increase in bubble growth in the evaporator and insufficient circulating power. The quality of each evaporator presents a very uneven distribution in Fig. 10(b). When the thermal flux reaches 40.8 kWm^{-2}, the quality of most evaporators has exceeded 0.5, with a fluctuation amplitude of approximately 20 %, which fully indicates that the difference in evaporation strength between each evaporator is relatively large.

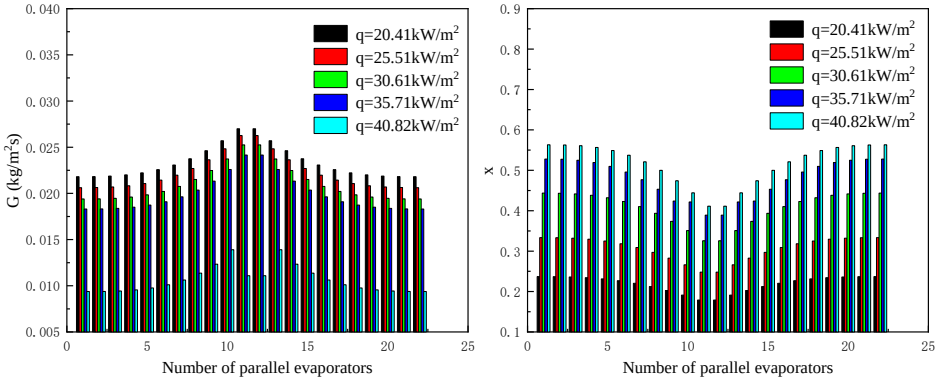

(a) Mass velocity (b) Quality

Fig. 10. Effect of the thermal flux on flow distribution

3.2.2 Effect of the branch diameter

The wall temperature distribution between parallel evaporators is relatively uniform in Fig. 11(a). This phenomenon indicates that branch diameter does not affect the temperature distribution. The reason is that the change of branch diameter has little effect on the heat transfer in the evaporator. In Fig. 11(b), the HTC shows different degrees of uneven distribution. The most significant uneven distribution occurs when the branch diameter is reduced to 8 mm. Moreover, when the branch diameter is reduced to 4 mm, the further decrease in the HTC results in a more uniform distribution between different evaporators. The HTC becomes a key factor limiting heat transfer.

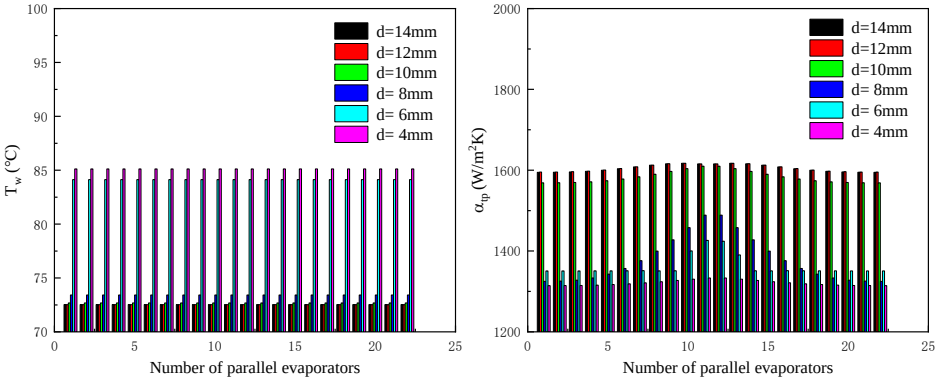

(a) Wall temperature (b) HTC

Fig. 11. Effect of the branch diameter on temperature distribution.

As the diameter of the branch decreases, different degrees of uneven distribution are observed between evaporators in Fig. 12(a). The branch diameters of 12 mm and 14 mm are relatively large flow maldistribution between evaporators. As the branch diameter decreases, the evaporator flow distribution becomes more uniform. The mass velocity approaches 0 $kgm^{-2}s$ at a diameter of 6 mm, indicating that the critical branch diameter of PECS has been reached. The quality shows a gradually uneven distribution of a gradually increasing phenomenon as the branch diameter increases in Fig. 12(b). When the branch diameter exceeds 8 mm, the outlet quality of each evaporator exhibits a highly uneven distribution. However, reducing the diameter to 6 mm results in a more uniform outlet quality distribution, accompanied by a rapid increase in evaporator outlet quality, reaching approximately 1. This sharp rise indicates a flow pattern transition from slug flow to mist flow in the evaporator.

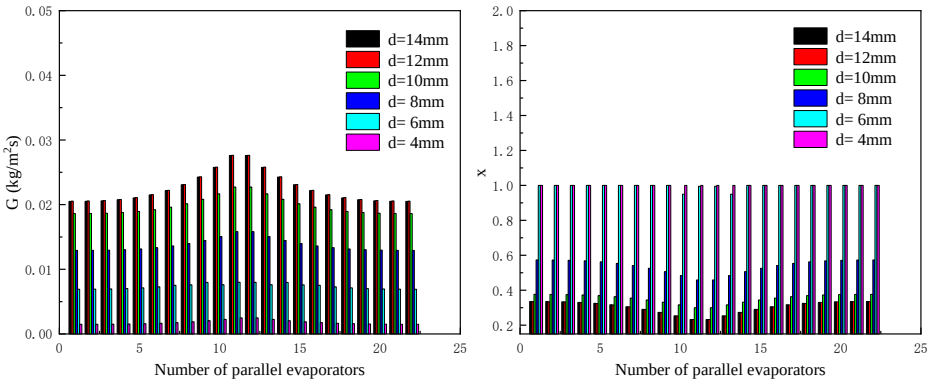

(a) Mass velocity (b) Quality

Fig. 12. Effect of the branch diameter on flow distribution.

3.2.3 Effect of the number of parallel evaporators

A relatively uniform temperature distribution is observed between evaporators in Fig. 13(a). The reason is that the strong heat transfer intensity in the evaporator ensures the uniform temperature distribution. Thus, this result indicates that increasing the number of parallel evaporators does not change the uniformity of temperature. When the number of parallel evaporators changes from 4 to 20, the distribution of HTC is relatively uniform in Fig. 13(b). It is noteworthy that the HTC exhibits a remarkably uneven distribution when the number of parallel evaporators increases to 24. This result indicates that the heat transfer in the evaporator distributed on both sides of the PECS begins to deteriorate. Therefore, 20 is the optimal number of parallel evaporators in the PECS.

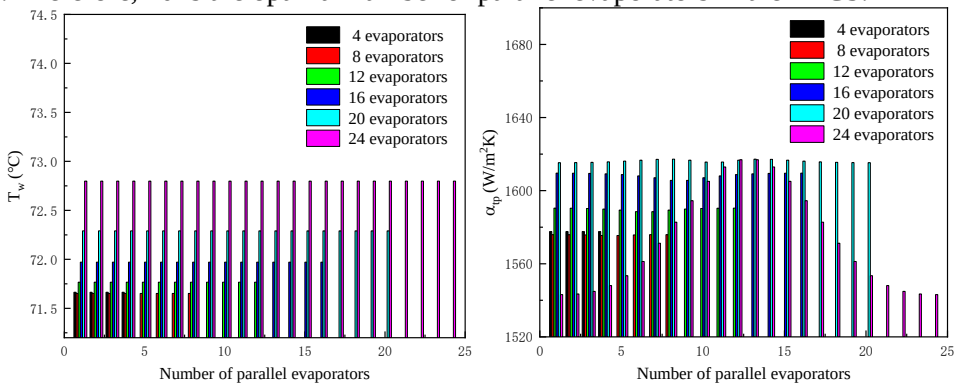

(a) Wall temperature (b) HTC

Fig.13. Effect of the number of parallel evaporators on temperature distribution.

When the number of parallel evaporators is less than 16, the flow distribution is relatively uniform in Fig. 14(a). Once the number of parallel evaporators exceeds 16, a noticeable uneven flow distribution becomes apparent. As the number of parallel evaporators increases to 24, the distribution becomes more uneven, with the maximum deviation between channels reaching 22.92 %. Hence, it is evident that the number of parallel evaporators significantly influences the flow distribution. The number of parallel evaporators increases, and the quality exhibits a gradual increase in Fig. 14(b). Upon reaching 24 parallel evaporators, the quality shows an apparent uneven distribution, with a maximum deviation of 27.03 %. The phenomenon indicates the formation of a mist flow pattern within the evaporator. Therefore, 24 parallel evaporators are the maximum number to ensure the uniform flow distribution of the PECS.

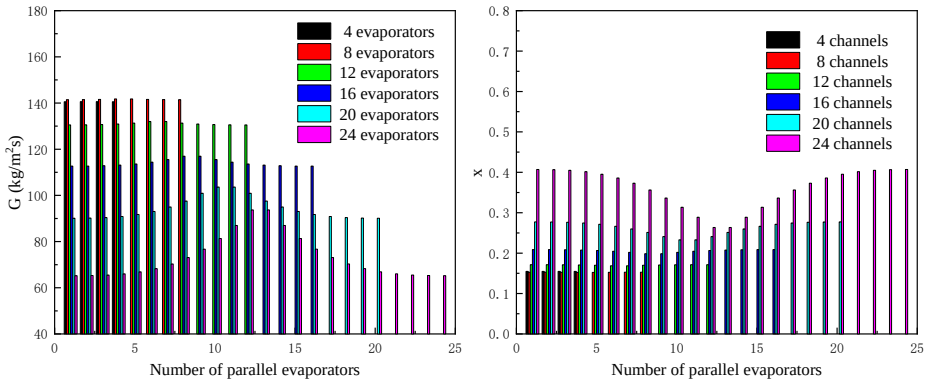

(a) Mass velocity (b) Quality

Fig.14. Effect of the number of parallel evaporators on flow distribution.

4. Conclusions

A novel coupling model of PECS for IGBT has been proposed, and the experimental setup of PECS is established to validate the accuracy of the proposed model. The thermohydraulic coupling performance of the PECS is analyzed from two-phase flow and heat transfer perspectives. The influence of the different boundary conditions on temperature and flow distribution of the PECS is thoroughly studied. The main conclusions of the study are as follows:

- The high thermal flux will change the flow pattern in the evaporator, which will lead to a wall temperature jump. The influence of thermal flux on wall temperature distribution is weak. However, the thermal flux has a great influence on the flow distribution, and the maximum deviation between evaporators is 30 %.
- When the branch diameter is 8 mm, the thermohydraulic performance of the system is optimal. The branch diameter does not affect the temperature distribution of PECS, while the branch diameter has a great influence on the flow distribution. The minimum critical branch diameter of the PECS for highly efficient operation is 6 mm.
- The number of parallel evaporators significantly influences the thermohydraulic performance. The number of parallel evaporators suitable for optimal thermohydraulic performance of PECS is less than 12. The 24 parallel evaporators are the maximum number to ensure the uniform flow distribution of the PECS.

Acknowledgment

The present research work has been funded by the Science Research Project of Hebei Education Department (BJK2024139) and the Innovation Fund of Hebei University of Engineering.

References

[1] Gong Z, Zang L, Wang G, et al. Thermal management implementation method for IGBT modules of inverters based on junction temperature estimation [J]. Journal of Power Electronics, 2024: 1-11.

[2] Zhang X, Tu C, Yan Y. Physics-informed neural network simulation of conjugate heat transfer in manifold microchannel heat sinks for high-power IGBT cooling [J]. International Communications in Heat Mass Transfer, 2024, 159: 108036.

[3] Qian G, Dou X, Lu G, et al. Parametric study and design of liquid cooling plates for high power density IGBT modules in wind power generation systems [J]. Thermal Science Engineering Progress, 2023, 43: 101992.

[4] Yang S, Guo X, Xu H, et al. Experimental study on the loop thermosyphon with a flat evaporator under different evaporator chamber thicknesses for IGBT cooling [J]. International Journal of Heat Mass Transfer, 2025, 240: 126682.

[5] Yoon S H, Saneie N, Kim Y J. Two-phase flow maldistribution in minichannel heat-sinks under non-uniform heating [J]. International Journal of Heat and Mass Transfer, 2014, 78: 527-37.

[6] Fang Y, Yang H, Huang Y, et al. Flow pattern maldistribution and manipulation during two-phase cooling for power batteries: A critical review [J]. Renewable Sustainable Energy Reviews, 2025, 211: 115362.

[7] Li W, Hrnjak P. Effect of liquid-vapor two-phase flow maldistribution on the thermal performance of brazed plate heat exchangers [J]. International Journal of Thermal Sciences, 2024, 205: 109292.
[8] Byun H, Kim N. Refrigerant distribution in a parallel flow heat exchanger having vertical headers and heated horizontal tubes [J]. Experimental Thermal and Fluid Science, 2011, 35(6): 920-32.
[9] Dario E, Tadrist L, Passos J. Review on two-phase flow distribution in parallel channels with macro and micro hydraulic diameters: Main results, analyses, trends [J]. Applied Thermal Engineering, 2013, 59(1-2): 316-35.
[10] Yin L, Wang Y, Jia L. Flow boiling instability of R134a in the large-area heat sink with interconnected parallel multi-minichannels [J]. International Journal of Thermal Sciences, 2024, 204: 109193.
[11] Zou Y, Hrnjak P S. Effects of fluid properties on two-phase flow and refrigerant distribution in the vertical header of a reversible microchannel heat exchanger–Comparing R245fa, R134a, R410A, and R32 [J]. Applied Thermal Engineering, 2014, 70(1): 966-76.
[12] Liu Y, Wang S. Distribution of gas-liquid two-phase slug flow in parallel micro-channels with different branch spacing [J]. International Journal of Heat and Mass Transfer, 2019, 132: 606-17.
[13] Huang Y, Wei C, Wang S, et al. Visualization study on the uniformity of refrigerant distribution in parallel multi-channels [J]. Applied Thermal Engineering, 2022, 213: 118804.
[14] Ki S, Lee J, Ryu S, et al. A bio-inspired, low pressure drop liquid cooling system for high-power IGBT modules for EV/HEV applications [J]. International Journal of Thermal Sciences, 2021, 161: 106708.
[15] Gao Z, Shang X, Bai J, et al. Study on the uneven flow distribution and non-uniform heat transfer in microchannels [J]. Applied Thermal Engineering, 2023, 230: 120824.
[16] Ablanque N, Oliet C, Rigola J, et al. Two-phase flow distribution in multiple parallel tubes [J]. International Journal of Thermal Sciences, 2010, 49(6): 909-21.
[17] Zhang T, Wen J T, Julius A, et al. Stability analysis and maldistribution control of two-phase flow in parallel evaporating channels [J]. International Journal of Heat and Mass Transfer, 2011, 54(25-26): 5298-305.
[18] Van Oevelen T, Weibel J A, Garimella S V. Predicting two-phase flow distribution and stability in systems with many parallel heated channels [J]. International Journal of Heat Mass Transfer, 2017, 107: 557-71.
[19] Xu W, Qi Z, Wang L, et al. Study of two-phase flow distribution in microchannel heat exchanger header-A numerical simulation [J]. International Journal of Thermofluids, 2022, 14: 100150.
[20] Qiao J X, Chen S Q, Liu S H, et al. Study on the prediction and optimization of flow mal-distribution in printed circuit heat exchangers based on machine learning [J]. Energy, 2024, 313: 134029.
[21] Hussein H A. A simulation study of thermal and hydraulic characteristics mini-channel circular heat sink: Effect of L-shaped multi-channel arrangement on flow maldistribution [J]. Case Studies in Thermal Engineering, 2025, 65: 105655.
[22] Saitoh S, Daiguji H, Hihara E. Correlation for boiling heat transfer of R-134a in horizontal tubes including effect of tube diameter [J]. International Journal of Heat and Mass Transfer, 2007, 50(25-26): 5215-25.
[23] Khodabandeh R. Pressure drop in riser and evaporator in an advanced two-phase thermosyphon loop [J]. International Journal of Refrigeration, 2005, 28(5): 725-34.
[24] Miropolskii Z, Snelobe P, Kalamesebe A. Void Fraction of water-steam mixture flow with or without heat transfer [J]. Teploenergetika, 1971, 5: 374-9.

Submitted: 13.2.2025.

Revised: 23.6.2025.

Accepted: 09.7.2025.